Waveguide Mode Solver Based On Neumann-to-Dirichlet Operators and Boundary Integral Equations[☆]

Wangtao Lu[a,b,c], Ya Yan Lu[c]

[a] *Joint Advanced Research Center of University of Science and Technology of China and City University of Hong Kong, Suzhou, Jiangsu, China*
[b] *School of Mathematical Sciences, University of Science and Technology of China, Hefei, Anhui, China*
[c] *Department of Mathematics, City University of Hong Kong, Kowloon, Hong Kong*

Abstract

For optical waveguides with high index-contrast and sharp corners, existing full-vectorial mode solvers including those based on boundary integral equations typically have only second or third order of accuracy. In this paper, a new full-vectorial waveguide mode solver is developed based on a new formulation of boundary integral equations and the so-called Neumann-to-Dirichlet operators for sub-domains of constant refractive index. The method uses the normal derivatives of the two transverse magnetic field components as the basic unknown functions, and it offers higher order of accuracy where the order depends on a parameter used in a graded mesh for handling the corners. The method relies on a standard Nyström method for discretizing integral operators and it does not require analytic properties of the electromagnetic field (which are singular) at the corners.

Keywords: Optical waveguide, waveguide mode solver, boundary integral equation, Neumann-to-Dirichlet operator.

[☆]This research was partially supported by a grant from City University of Hong Kong (Project No. 7008107).

Email addresses: luwan@mail.ustc.edu.cn (Wangtao Lu), mayylu@cityu.edu.hk (Ya Yan Lu)

1. Introduction

Optical waveguides [1, 2, 3] are structures that guide the propagation of light. They are the fundamental components in communications systems and integrated optical circuits. In recent years, many optical waveguides with complicated structures have appeared. For example, photonic crystal fibers and plasmonic waveguides have been extensively studied due to their many unique properties which are not available in traditional waveguides. Although many numerical methods have been developed for analyzing optical waveguides, accurate numerical simulations for some recently developed optical waveguides remain time consuming.

For a given optical waveguide, the most important mathematical problem is to calculate its guided modes which propagate along the waveguide axis. For an optical waveguide with its axis in the z direction, a guided mode is a special solution of the Maxwell's equations where the electromagnetic fields depend on z as $e^{i\beta z}$ for a real constant β (the so-called propagation constant). This is an eigenvalue problem formulated on the plane perpendicular to the waveguide axis (i.e., the xy plane), where β^2 is the eigenvalue. For waveguides with high index-contrast, sharp corners and complex micro-structures, analytic approximations leading to scalar or semi-vectorial models are no longer valid, a rigorous full-vectorial analysis based on the Maxwell's equations is needed. Numerical methods that discretize the cross section of the waveguide give rise to linear matrix eigenvalue problems. The discretization can be obtained by the finite difference method [4, 5, 6, 7, 8, 9, 10, 11, 12], the finite element method [13, 14, 15, 16, 17, 18, 19, 20], the multi-domain pseudospectral method [21, 22, 23], etc. The resulting matrices are often very large, and the matrix eigenvalue problem can only be solved by iterative methods and the accuracy may be limited.

A different approach is to formulate a nonlinear eigenvalue problem

$$F(\beta)\boldsymbol{\phi} = 0 \tag{1}$$

where F is a much smaller square matrix. The propagation constant β is determined from the condition that the matrix $F(\beta)$ is a singular. Numerical methods using this nonlinear approach include the film mode matching method [24, 25, 26, 27, 28], the multipole method [29, 30, 31, 32, 33, 34] and the boundary integral equation (BIE) method [35, 36, 37, 38, 39, 40], etc. The film mode matching is quite successful, but it is only applicable to waveguides with vertical and horizontal refractive index discontinuities.

The multipole method is accurate for photonic crystal fibers with circular inclusions, but it cannot be easily extended to other optical waveguides. The BIE method is more general. Its only restriction is that the refractive index has to be piecewise constant.

Dielectric corners are the main source of difficulty for waveguide mode solvers, since electromagnetic fields can diverge at the corners [41, 42, 43, 44]. For the finite difference method, much effort has been devoted to accurate discretization at the corners [8, 11]. For the finite element method, careful mesh refinements near the corners are necessary. For the BIE method, Lu and Yevick [37, 38] developed boundary element discretizations that take special care of the corner singularity based on analytic properties of the electromagnetic fields at the corners, but their numerical results only reveal a second order of accuracy.

In this paper, we develop a new high order full-vectorial BIE waveguide mode solver which is relatively simple to implement and gives accurate results. Our method uses BIEs to calculate the so-called Neumann-to-Dirichlet (NtD) operators for sub-domains of constant refractive index. The integral operators are discretized by a Nyström method with a graded mesh technique to take care of the corners. Unlike some BIE formulations, our method is applicable to optical waveguides in integrated optics where the background is usually a layered medium.

2. Eigenvalue problem

We consider a dielectric waveguide characterized by a z-independent refractive index function $n = n(x, y)$, where $\{x, y, z\}$ is a Cartesian coordinate system, z is the variable along the waveguide axis, x and y are the transverse variables, and n is real positive and piecewise constant. For time-harmonic waves that depend on time as $\exp(-i\omega t)$, where ω is the angular frequency, the governing equations are the following Maxwell's equations:

$$\nabla \times \boldsymbol{E} = ik_0 \boldsymbol{H}, \quad \nabla \times \boldsymbol{H} = -ik_0 \varepsilon \, \boldsymbol{E}. \tag{2}$$

In the above, $\boldsymbol{E}$ is the electric field, $\boldsymbol{H}$ is the magnetic field (multiplied by the free space impedance), $k_0 = \omega/c_0$ is the free space wavenumber, c_0 is the speed of light in vacuum, and $\varepsilon = n^2$ is the relative permittivity or dielectric function. A waveguide mode is a special solution of (2), such that $\boldsymbol{E}$ and $\boldsymbol{H}$ depend on z as $\exp(i\beta z)$ for a constant β (the propagation constant). For a guided mode, β is real, and $\boldsymbol{E}$ and $\boldsymbol{H}$ tend to zero as $r = \sqrt{x^2 + y^2} \to \infty$.

The Maxwell's equations give rise to eigenvalue problems for waveguide modes. If the two transverse components of the magnetic field are used, the eigenvalue problem is

$$\begin{bmatrix} \mathcal{A}_{11} & \mathcal{A}_{12} \\ \mathcal{A}_{21} & \mathcal{A}_{22} \end{bmatrix} \begin{bmatrix} H_y \\ -H_x \end{bmatrix} = \beta^2 \begin{bmatrix} H_y \\ -H_x \end{bmatrix}, \tag{3}$$

where H_x and H_y are the x and y components of $\boldsymbol{H}$, $\mathcal{A}_{11}$, $\mathcal{A}_{12}$, $\mathcal{A}_{21}$ and $\mathcal{A}_{22}$ are differential operators given by

$$\mathcal{A}_{11} = \varepsilon\partial_x(\varepsilon^{-1}\partial_x\,\cdot) + \partial_y^2 + k_0^2\varepsilon, \tag{4}$$

$$\mathcal{A}_{12} = \varepsilon\partial_x(\varepsilon^{-1}\partial_y\,\cdot) - \partial_{xy}^2, \tag{5}$$

$$\mathcal{A}_{21} = \varepsilon\partial_y(\varepsilon^{-1}\partial_x\,\cdot) - \partial_{yx}^2, \tag{6}$$

$$\mathcal{A}_{22} = \varepsilon\partial_y(\varepsilon^{-1}\partial_y\,\cdot) + \partial_x^2 + k_0^2\varepsilon. \tag{7}$$

When the xy plane (perpendicular to the waveguide axis) is properly truncated and discretized, Eq. (3) leads to a linear matrix eigenvalue problem, where β^2 is the eigenvalue, but the involved matrices are often very large.

The BIE method is applicable to waveguides with piecewise constant refractive index profiles. Most optical waveguides appeared in applications indeed have piecewise constant refractive indices, since they are engineered structures. For a waveguide mode with propagation constant β and in a domain Ω of constant refractive index n (relative permittivity $\varepsilon = n^2$), all six components of the electromagnetic fields satisfy the Helmholtz equation:

$$\partial_x^2 u + \partial_y^2 u + \eta\, u = 0 \quad \text{for } (x, y) \in \Omega, \tag{8}$$

where $\eta = k_0^2\varepsilon - \beta^2$. Notice that η is positive in the waveguide core, and it is usually negative outside the core. In the latter case, Eq. (8) becomes the modified Helmholtz equation. In existing full-vectorial BIE formulations, the two z components of the electromagnetic fields, E_z and H_z, are used, then along a dielectric interface Γ, it is necessary to enforce the continuity of

$$\frac{\varepsilon}{\eta}\partial_{\boldsymbol{\nu}} E_z + \frac{\beta}{k_0\eta}\partial_{\boldsymbol{\tau}} H_z \quad \text{and} \quad \frac{1}{\eta}\partial_{\boldsymbol{\nu}} H_z - \frac{\beta}{k_0\eta}\partial_{\boldsymbol{\tau}} E_z, \tag{9}$$

where $\boldsymbol{\nu} = (\nu_x, \nu_y)$ is a unit normal vector, $\boldsymbol{\tau} = (-\nu_y, \nu_x)$ is a unit tangential vector, $\partial_{\boldsymbol{\nu}}$ and $\partial_{\boldsymbol{\tau}}$ are normal and tangential derivative operators along Γ.

In domain Ω, both E_z and H_z satisfies the Helmholtz equation (8). On the boundary of domain Ω, denoted as $\partial\Omega$, if we first calculate the Dirichlet-to-Neumann (DtN) map Λ such that $\Lambda u = \partial_{\boldsymbol{\nu}} u$ on $\partial\Omega$ for any u satisfying (8),

then $\partial_{\boldsymbol{\nu}} E_z$ and $\partial_{\boldsymbol{\nu}} H_z$ can be expressed in terms of E_z and H_z, respectively. However, for domains with corners, accurate matrix approximations of the DtN maps are difficult to obtain. Our approach is based on the inverse of DtN map, namely, the Neumann-to-Dirichlet (NtD) map $\mathcal{N}$. The operator $\mathcal{N}$ satisfies

$$\mathcal{N}\partial_{\boldsymbol{\nu}} u = u \quad \text{on} \quad \partial\Omega, \tag{10}$$

where u is any solution of Eq. (8). If we consider $\partial_{\boldsymbol{\nu}} E_z$ and $\partial_{\boldsymbol{\nu}} H_z$ as the unknown functions defined on $\partial\Omega$, then $E_z = \mathcal{N}\partial_{\boldsymbol{\nu}} E_z$, $H_z = \mathcal{N}\partial_{\boldsymbol{\nu}} H_z$, and the two functions in (9) can also be evaluated if the tangential derivative operator is approximated.

We prefer to use the normal derivatives of the two transverse magnetic field components, i.e., $\phi_x = \partial_{\boldsymbol{\nu}} H_x$ and $\phi_y = \partial_{\boldsymbol{\nu}} H_y$, as the unknown functions on $\partial\Omega$, since H_x and H_y are the smoothest functions among the six components [8]. We choose to impose the interface conditions from the continuities of H_x, H_y, H_z and E_z. The transverse electric field components E_x and E_y are intentionally avoided, since they always diverge at the corners. If ϕ_x and ϕ_y are given, the two transverse magnetic field components can be easily evaluated by the NtD map:

$$H_x = \mathcal{N}\phi_x, \quad H_y = \mathcal{N}\phi_y. \tag{11}$$

The two z components are related to the derivatives of H_x and H_y. Since the magnetic field $\boldsymbol{H}$ is divergence free, we have

$$\partial_x H_x + \partial_y H_y + i\beta H_z = 0. \tag{12}$$

From the z component of the curl $\boldsymbol{H}$ equation in (2), we obtain

$$ik_0\varepsilon E_z = \partial_y H_x - \partial_x H_y. \tag{13}$$

Re-writing the partial derivatives with respect to x and y as linear combinations of the normal and tangential derivatives, we have

$$ik_0\varepsilon E_z = \nu_y\partial_{\boldsymbol{\nu}} H_x + \nu_x\partial_{\boldsymbol{\tau}} H_x - \nu_x\partial_{\boldsymbol{\nu}} H_y + \nu_y\partial_{\boldsymbol{\tau}} H_y, \tag{14}$$

$$-i\beta H_z = \nu_x\partial_{\boldsymbol{\nu}} H_x - \nu_y\partial_{\boldsymbol{\tau}} H_x + \nu_y\partial_{\boldsymbol{\nu}} H_y + \nu_x\partial_{\boldsymbol{\tau}} H_y, \tag{15}$$

where ν_x and ν_y are the components of the unit normal vector. We introduce a matrix operator $\mathcal{M}$ (the magnetic transverse-to-longitudinal (TtL) operator)

that maps the transverse magnetic field components to the two z components (the longitudinal components), that is,

$$\begin{bmatrix} E_z \\ H_z \end{bmatrix} = \mathcal{M} \begin{bmatrix} \phi_x \\ \phi_y \end{bmatrix}. \tag{16}$$

From Eqs. (14) and (15), we obtain

$$\mathcal{M} = \begin{bmatrix} ik_0\varepsilon & \\ & -i\beta \end{bmatrix}^{-1} \begin{bmatrix} \nu_y + \nu_x\mathcal{D}, & -\nu_x + \nu_y\mathcal{D} \\ \nu_x - \nu_y\mathcal{D}, & \nu_y + \nu_x\mathcal{D} \end{bmatrix}, \tag{17}$$

where $\mathcal{D} = \partial_{\boldsymbol{\tau}} \circ \mathcal{N}$ is the composition of the NtD map with the tangential derivative operator. Clearly, if the tangential derivative operator is approximated, $\mathcal{M}$ can be easily evaluated.

To establish a nonlinear eigenvalue problem, we divide the xy plane (which may be truncated) into domains of constant refractive index, assuming that the boundaries of these domains are piecewise smooth. The simplest kind of optical waveguides consists of a high-index core embedded in a low-index surrounding medium. For such a waveguide, the xy plane is divided into two domains: a bounded domain for the waveguide core and an unbounded domain for the surrounding medium. An example involving a trapezoidal core is shown in Fig. 1(a). For waveguides with a layered sur-

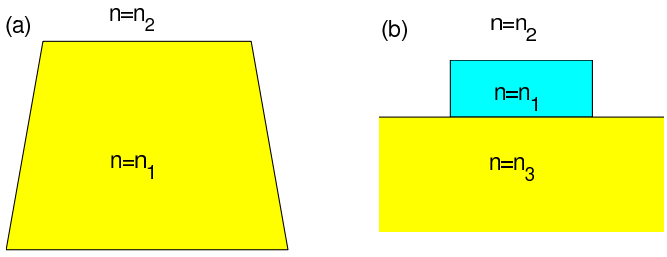

Figure 1: Optical waveguides with a waveguide core surrounded by a homogeneous medium (a) or a layered medium (b).

rounding medium, the xy plane is first truncated and then divided into a number of domains. As an example, a rectangular waveguide on top of one medium and covered by a different medium is shown in Fig. 1(b). In that case, the xy plane is truncated and divided into three domains. The boundaries of all these domains consist of a few smooth segments. The trapezoidal waveguide shown in Fig. 1(a) has four boundary segments. The truncated

domain for the rectangular waveguide shown in Fig. 1(b) has six interior boundary segments and two exterior boundary segments. The six interior boundary segments consist of four segements for the boundary of the rectangular core, and two segments for the horizontal interface between the top and bottom media of refactive indices n_2 and n_3. Notice that the entire horizontal interface on top of the n_3 medium is broken into three segments. The two exterior segments are the boundary segements in the upper and lower planes for the domains with refractive indices n_2 and n_3, respectively. For truncating the xy plane, the exterior boundary segments should be sufficiently far away from the waveguide core, so that both ϕ_x and ϕ_y can be approximated by zero. Each interior boundary segment is shared by two neighboring domains. Since ϕ_x and ϕ_y are usually not continuous on dielectric interfaces, we have four unknown functions ϕ_x^+, ϕ_y^+, ϕ_x^- and ϕ_y^- on an interior segment, where the superscripts denote one-sided limits. On each interior boundary segment, we establish four equations based on the continuity of H_x, H_y, H_z and E_z using the NtD and magnetic TtL operators of the two neighboring domains. All these equations give rise to the system (1), where $\boldsymbol{\phi}$ denotes ϕ_x^+, ϕ_y^+, ϕ_x^- and ϕ_y^- on all interior boundary segments.

In our actual numerical implementation, the procedure given above is slightly modified to produce a more stable method. The details are given in Section 5.

3. Neumann-to-Dirichlet map

For a domain Ω with a constant refractive index n and a piecewise smooth boundary $\partial\Omega$, an accurate numerical method is available for computing its NtD map $\mathcal{N}$ [45]. The method uses a boundary integral equation, discretizes the integral operators by a Nyström method and works on a graded mesh when Ω has corners. We summarize the key steps of this method in this section.

If u satisfies the Helmholtz equation (8) in Ω and if the boundary $\partial\Omega$ is smooth, then u and $\partial_{\boldsymbol{\nu}} u$ satisfy the following boundary integral equation

$$(1 + \mathcal{K})u = \mathcal{S}\,\partial_{\boldsymbol{\nu}} u \quad \text{on} \quad \partial\Omega, \tag{18}$$

where $\boldsymbol{\nu}$ is an outward normal vector of $\partial\Omega$, $\mathcal{S}$ and $\mathcal{K}$ are boundary integral operators defined as

$$(\mathcal{S}\psi)(\boldsymbol{r}) \;=\; 2\int_{\partial\Omega} G(\boldsymbol{r},\tilde{\boldsymbol{r}})\psi(\tilde{\boldsymbol{r}})\,ds(\tilde{\boldsymbol{r}}), \quad \boldsymbol{r} \in \partial\Omega, \tag{19}$$

$$(\mathcal{K}\psi)(\boldsymbol{r}) \;=\; 2\int_{\partial\Omega} \frac{\partial G(\boldsymbol{r},\tilde{\boldsymbol{r}})}{\partial\nu(\tilde{\boldsymbol{r}})}\psi(\tilde{\boldsymbol{r}})\,ds(\tilde{\boldsymbol{r}}), \quad \boldsymbol{r}\in\partial\Omega, \tag{20}$$

G is the Green's function of the Helmholtz equation

$$G(\boldsymbol{r},\tilde{\boldsymbol{r}}) = \frac{i}{4}H_0^{(1)}(\sqrt{\eta}|\boldsymbol{r}-\tilde{\boldsymbol{r}}|), \quad \boldsymbol{r}\neq\tilde{\boldsymbol{r}}, \tag{21}$$

$H_0^{(1)}$ is a Hankel function, $\boldsymbol{r} = (x, y)$ and $\tilde{\boldsymbol{r}} = (\tilde{x}, \tilde{y})$. From (18), we can calculate the NtD map by $\mathcal{N} = (1+\mathcal{K})^{-1}\mathcal{S}$.

The integral operators $\mathcal{S}$ and $\mathcal{K}$ can be discretized by a Nyström method as described in [46]. If $\partial\Omega$ has parametric representation

$$\boldsymbol{r}(\gamma) = [x(\gamma), y(\gamma)], \quad 0\le\gamma\le L, \tag{22}$$

then Eq. (18) can be transformed to

$$u(\gamma) + \int_0^L K(\gamma,\tilde{\gamma})u(\tilde{\gamma})d\tilde{\gamma} = \int_0^L S(\gamma,\tilde{\gamma})\partial_{\boldsymbol{\nu}}u(\tilde{\gamma})d\tilde{\gamma}, \tag{23}$$

for two kernel functions K and S, where $u(\gamma)$ and $\partial_{\boldsymbol{\nu}}u(\gamma)$ denote $u(\boldsymbol{r}(\gamma))$ and $\partial_{\boldsymbol{\nu}}u(\boldsymbol{r}(\gamma))$, respectively. To discretize Eq. (23), we split each kernel as the sum of a smooth part and a part with a simpler logarithmic singularity, then evaluate them by the trapezoidal rule and the quadrature formula of Martensen and Kussmaul [46, 47, 48] respectively, based on a uniform discretization of γ. This leads to matrix approximations for $\mathcal{S}$ and $\mathcal{K}$, and therefore $\mathcal{N}$. When Ω is not the waveguide core and η in Eq. (8) is negative, it is necessary to modify the above kernel-splitting technique to avoid numerical instabilities caused by some exponentially growing terms [35].

If $\partial\Omega$ is piecewise smooth, then Eq. (18) should be revised as

$$(\theta/\pi + \mathcal{K})u = \mathcal{S}\,\partial_{\boldsymbol{\nu}}u \quad \text{on} \quad \partial\Omega, \tag{24}$$

where $\theta = \theta(\boldsymbol{r})$ is the interior angle of Ω at $\boldsymbol{r}\in\partial\Omega$. If $\partial\Omega$ has a few corners, then $\theta(\boldsymbol{r})\neq\pi$ only at these corners. To avoid the discontinuous function $\theta(\boldsymbol{r})$, we follow [46, 49], consider the Laplace equation $\partial_x^2u_0 + \partial_y^2u_0 = 0$ and the related boundary integral equation

$$(\theta/\pi + \mathcal{K}_0)u_0 = \mathcal{S}_0\,\partial_{\boldsymbol{\nu}}u_0 \quad \text{on} \quad \partial\Omega, \tag{25}$$

where $\mathcal{S}_0$ and $\mathcal{K}_0$ are defined as $\mathcal{S}$ and $\mathcal{K}$ with G replaced by

$$G_0(\boldsymbol{r},\tilde{\boldsymbol{r}}) = \frac{-1}{2\pi}\ln|\boldsymbol{r}-\tilde{\boldsymbol{r}}|, \quad \boldsymbol{r}\neq\tilde{\boldsymbol{r}}. \tag{26}$$

In particular, if we choose $u_0 = 1$, then

$$\theta/\pi + \mathcal{K}_0 1 = 0 \quad \text{on} \quad \partial\Omega, \tag{27}$$

where $\mathcal{K}_0 1$ is a function defined on $\partial\Omega$ and it is obtained by applying $\mathcal{K}_0$ on the constant function 1. Replacing θ/π by $-\mathcal{K}_0 1$ in Eq. (24), we obtain

$$(\mathcal{K} - \mathcal{K}_0 1)u = \mathcal{S}\partial_{\boldsymbol{\nu}} u \quad \text{on} \quad \partial\Omega. \tag{28}$$

Therefore, the NtD map is given by $\mathcal{N} = (\mathcal{K} - \mathcal{K}_0 1)^{-1}\mathcal{S}$. If Ω is the exterior of a bounded domain, we need to re-write the boundary integral equation of the Laplace equation for a domain between $\partial\Omega$ and a large circle. This leads to

$$(\mathcal{K} - \mathcal{K}_0 1 - 2)u = \mathcal{S}\partial_{\boldsymbol{\nu}} u \quad \text{on} \quad \partial\Omega. \tag{29}$$

In that case, the NtD map is given by $\mathcal{N} = (\mathcal{K} - \mathcal{K}_0 1 - 2)^{-1}\mathcal{S}$.

One way to take care of the singularities at the corners is to use a graded mesh such that the new integrands are smooth up to certain order, and then apply the same Nyström method and quadrature formulae [46, 49, 50]. The graded mesh corresponds to a scaling function $\gamma = w(\zeta)$ and a uniform discretization in ζ, where γ is the original parameter in the parametric representation (22). Let the corners be given by $\boldsymbol{r}_j = \boldsymbol{r}(\gamma_j)$ for $0 \le j \le j_*$, where $\gamma_0 = 0$ and $\gamma_{j_*} = L$ correspond to the same corner, then the scaling function is

$$w(\zeta) = \frac{\gamma_{j+1} w_1^p + \gamma_j w_2^p}{w_1^p + w_2^p} \quad \text{for} \quad \zeta^{(j)} \le \zeta \le \zeta^{(j+1)}, \quad j = 0, 1, ..., j_* - 1,$$

where $\zeta^{(j)}$ corresponds to a corner point, i.e., $\gamma_j = w(\zeta^{(j)})$, and

$$w_1 = \left(\frac{1}{2} - \frac{1}{p}\right)\xi^3 + \frac{\xi}{p} + \frac{1}{2}, \quad w_2 = 1 - \omega_1, \quad \xi = \frac{2\zeta - [\zeta^{(j)} + \zeta^{(j+1)}]}{\zeta^{(j+1)} - \zeta^{(j)}}.$$

The integer p is the graded mesh order. The derivatives of w up to order $p-1$ vanish at the corner points. When ζ is uniformly discretized on the interval $[\zeta^{(j)}, \zeta^{(j+1)}]$, the corresponding points of γ are densely distributed near γ_j and γ_{j+1}. However, the maximum derivative of w is just $2(\gamma_{j+1} - \gamma_j)/[\zeta^{(j+1)} - \zeta^{(j)}]$, which is obtained at the midpoint $[\zeta^{(j)} + \zeta^{(j+1)}]/2$. Therefore, the discretization points of γ will not be widely separated even when p is large. Assuming that $\zeta^{(0)} = 0$ and $\zeta^{(j_*)} = \tilde{L}$, the parameter ζ is then discretized

uniformly as $\zeta_k = k\tilde{L}/N$ for an integer N and $0 \le k \le N$. In particular, we assume that all corner points, $\zeta^{(j)}$ for $0 \le j < j_*$, are discretization points of ζ. Based on the graded mesh and the Nyström method, we can approximate $\mathcal{S}$, $\mathcal{K}$ and $\mathcal{K}_0$ by matrices and then find the NtD map $\mathcal{N}$. Notice that $\mathcal{K}_0 1$ in Eq. (29) corresponds to a diagonal matrix where the diagonal elements are the row sums of the matrix $\mathcal{K}_0$.

4. Tangential derivative

In section 2, we introduced an operator $\mathcal{M}$ that links the normal derivatives of transverse magnetic field components and the z components, and it depends on the NtD map $\mathcal{N}$ and the tangential derivative operator $\partial_{\boldsymbol{\tau}}$. Let $u(\boldsymbol{r})$ be a function defined on $\partial\Omega$, for the original parametric representation (22) and if $\boldsymbol{r}(\gamma)$ is not a corner point, the tangential derivative is given by

$$\partial_{\boldsymbol{\tau}} u(\boldsymbol{r}(\gamma)) = \frac{1}{|\boldsymbol{r}'(\gamma)|} \frac{du(\boldsymbol{r}(\gamma))}{d\gamma}, \tag{30}$$

where $|\boldsymbol{r}'(\gamma)| = \sqrt{[x'(\gamma)]^2 + [y'(\gamma)]^2}$. When the graded mesh is used through the substitution $\gamma = w(\zeta)$, the tangential derivative is given by

$$\partial_{\boldsymbol{\tau}} u(\boldsymbol{r}(w(\zeta)) = \frac{1}{|\boldsymbol{r}'(w(\zeta))|\, w'(\zeta)} \frac{du(\boldsymbol{r}(w(\zeta)))}{d\zeta}. \tag{31}$$

To simplify the notations, we denote $u(\boldsymbol{r}(w(\zeta)))$ by $u(\zeta)$. Since $u(\zeta)$ is periodic in ζ and we are given $u(\zeta_k)$ for $0 \le k < N$ based on a uniform discretization of ζ, we can approximate $du/d\zeta$ through an approximate Fourier series of $u(\zeta)$. More specifically, if N is an even integer, we have

$$u(\zeta) \approx \sum_{l=-N/2}^{N/2-1} \hat{u}_l \exp(i2\pi l\zeta/\tilde{L}), \tag{32}$$

where the coefficients are calculated from the discrete Fourier transform

$$\hat{u}_l = \frac{1}{N} \sum_{k=0}^{N-1} u(\zeta_k) \exp(-i2\pi lk/N), \quad -\frac{N}{2} \le l < \frac{N}{2}. \tag{33}$$

Therefore, we can evaluate $du/d\zeta$ at the N points by

$$\frac{du}{d\zeta}(\zeta_k) \approx \sum_{l=-N/2}^{N/2-1} \frac{i2\pi l}{\tilde{L}} \hat{u}_l \exp(i2\pi lk/N), \quad k = 0, 1, ..., N-1. \tag{34}$$

This leads to a differentiation matrix $\mathcal{D}_\zeta$, such that

$$\frac{d\boldsymbol{u}}{d\zeta} \approx \mathcal{D}_\zeta \boldsymbol{u}, \tag{35}$$

where $\boldsymbol{u}$ is a column vector of length N for $u(\zeta_k)$, $0 \le k < N$. The case for an odd integer N is similar.

At a corner, the tangential derivative does not exist. This is reflected by the fact that $w' = 0$ and $du/d\zeta = 0$ at the corner, thus formula (31) is no longer applicable. Meanwhile, some points in the graded mesh are very close to the corners, and w' for these points are extremely small. Formula (31) for the tangential derivative involves a division by $w'(\zeta)$ which amplifies round-off error and induces numerical instability. We propose an alternative formulation in the next section.

5. Improved formulation

To develop a numerically more stable method, we replace the two basic functions ϕ_x and ϕ_y (the normal derivatives of H_x and H_y) by

$$\tilde{\phi}_x = w'\partial_{\boldsymbol{\nu}} H_x, \quad \tilde{\phi}_x = w'\partial_{\boldsymbol{\nu}} H_y, \tag{36}$$

where $w(\zeta)$ is the scaling function used to define the graded mesh. On interfaces between different domains of constant refractive index, we impose the continuity of H_x, H_y, $w'E_z$ and $w'H_z$. Therefore, we need to revise the NtD map $\mathcal{N}$ and the magnetic TtL operator $\mathcal{M}$.

For the integral operator $\mathcal{S}$ given in (19), when the parametric representation (22) and the scaling $\gamma = w(\zeta)$ is used, we have

$$ds(\boldsymbol{r}) = |\boldsymbol{r}'(\gamma)|\, d\gamma = |\boldsymbol{r}'(w(\zeta))| w'(\zeta)\, d\zeta.$$

Therefore, there is an operator $\tilde{\mathcal{S}}$, such that $\mathcal{S}\psi = \tilde{\mathcal{S}}(w'\psi)$. If we use this relation in boundary integral equation (29), we obtain a modified NtD map $\tilde{\mathcal{N}}$, such that $\tilde{\mathcal{N}}(w'\partial_{\boldsymbol{\nu}} u) = u$. Therefore for H_x and H_y, we have

$$H_x = \tilde{\mathcal{N}}\tilde{\phi}_x, \quad H_y = \tilde{\mathcal{N}}\tilde{\phi}_y. \tag{37}$$

For the tangential derivative, we multiply w' to both sides of (31) and obtain

$$w'\partial_{\boldsymbol{\tau}} u = |\boldsymbol{r}'|^{-1}\partial_\zeta u. \tag{38}$$

This leads to

$$w'\partial_{\boldsymbol{\tau}} H_x = \tilde{\mathcal{D}}\tilde{\phi}_x, \quad w'\partial_{\boldsymbol{\tau}} H_y = \tilde{\mathcal{D}}\tilde{\phi}_y, \tag{39}$$

where $\tilde{\mathcal{D}} = |\boldsymbol{r}'|^{-1}\partial_\zeta \circ \tilde{\mathcal{N}}$. Meanwhile, multiplying w' to Eqs. (14) and (15), we obtain

$$\begin{bmatrix} w'E_z \\ w'H_z \end{bmatrix} = \tilde{\mathcal{M}} \begin{bmatrix} \tilde{\phi}_x \\ \tilde{\phi}_y \end{bmatrix}, \tag{40}$$

where

$$\tilde{\mathcal{M}} = \begin{bmatrix} ik_0\varepsilon & \\ & -i\beta \end{bmatrix}^{-1} \begin{bmatrix} \nu_y + \nu_x\tilde{\mathcal{D}}, & -\nu_x + \nu_y\tilde{\mathcal{D}} \\ \nu_x - \nu_y\tilde{\mathcal{D}}, & \nu_y + \nu_x\tilde{\mathcal{D}} \end{bmatrix}. \tag{41}$$

From Eqs. (37) and (40), we can express H_x, H_y, $w'E_z$ and $w'H_z$ in terms of $\tilde{\phi}_x$ and $\tilde{\phi}_y$ on the boundary of the domain Ω. When the transverse plane of the optical waveguide is divided into a number of domains with constant refractive index, we set up four equations on each interior boundary segment that separates two domains. These four equations come from the continuity of H_x, H_y, $w'E_z$ and $w'H_z$, and they are related to $\tilde{\phi}_x$ and $\tilde{\phi}_y$ of these two domains. Since $\tilde{\phi}_x$ and $\tilde{\phi}_y$ are usually not continuous across a dielectric interface, we have four unknown functions $\tilde{\phi}_x^{\pm}$ and $\tilde{\phi}_y^{\pm}$ on each boundary segments, where the superscripts represent one-sided limits from the two domains in different sides of the segment. All these equations give rise to the system (1), where $\boldsymbol{\phi}$ represents $\tilde{\phi}_x^{\pm}$ and $\tilde{\phi}_y^{\pm}$ on all interior boundary segments.

In the fully discrete case, $\partial\Omega$ is sampled at N points corresponding to a uniform discretization of ζ, that is, ζ_k for $0 \le k < N$. The modified NtD map $\tilde{\mathcal{N}}$ is represented by an $N \times N$ matrix. Notice that these N points in the graded mesh include a total of j_* corners points where $w' = 0$. For (37), if we remove the corner points, $\tilde{\phi}_x$, $\tilde{\phi}_y$, H_x and H_y become column vectors of length $N - j_*$ and $\tilde{\mathcal{N}}$ becomes an $(N - j_*) \times (N - j_*)$ matrix. The case for (40) and (41) is similar. Before the removal of corner points, $\tilde{\mathcal{D}}$ is the product of three $N \times N$ matrices: the diagonal matrix with entries $1/|\boldsymbol{r}'(w(\zeta_k))|$, the differentiation matrix $\mathcal{D}_\zeta$ given in Section 4, and the matrix form of the modified NtD map $\tilde{\mathcal{N}}$. After the corner points are removed, $w'E_z$ and $w'H_z$ are represented by column vectors of length $N - j_*$, $\tilde{\mathcal{D}}$ becomes an $(N-j_*)\times(N-j_*)$ matrix and $\mathcal{M}$ becomes a $2(N-j_*)\times 2(N-j_*)$ matrix. In (41), ν_x and ν_y are represented by diagonal matrices of size $(N-j_*)\times(N-j_*)$, $ik_0\varepsilon$ and $-i\beta$ should each multiply an $(N - j_*) \times (N - j_*)$ identity matrix.

To solve the nonlinear eigenvalue problem (1), we search the propagation constant β from

$$\sigma_1(F(\beta)) = 0, \tag{42}$$

where σ_1 is the smallest singular value of the matrix $F(\beta)$. If an good initial guess for β is not known, a searching method developed by Hochman and Leviatan [51] can be used. The method involves the generalized singular value decomposition for a pair of matrices $F(\beta)$ and $\tilde{F}(\beta)$, where $\tilde{F}(\beta)$ is obtained from $F(\beta)$ and its effect is to make the physically correct waveguide mode more dominant.

6. Numerical Examples

In this section, we illustrate our method by a few numerical examples. First, we consider a bounded waveguide previously analyzed by a number of authors [8, 11, 23]. The waveguide cross section is a 1μm $\times$ 1μm square shown in Fig. 2(a), where the refractive indices of the lower left corner (a 0.5μm

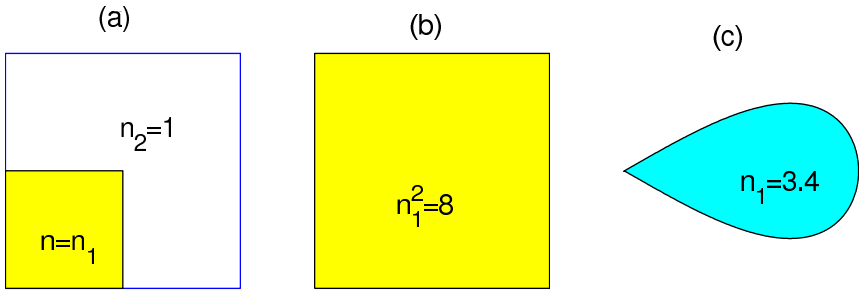

Figure 2: (a) A bounded waveguide, (b) an open square waveguide, (c) an open waveguide with a drop-shaped core.

$\times$ 0.5μm square) and the other region are n_1 and $n_2 = 1$, respectively. We consider two cases: (1) $n_1 = 1.5$, and (2) $n_1 = \sqrt{8}$. The boundary conditions are $H_x = 0$ and $\partial_{\boldsymbol{\nu}} H_y = 0$, and they correspond to perfectly electric conductor vertical boundaries and perfectly magnetic conductor horizontal boundaries. For the two domains Ω_1 and Ω_2 with indices n_1 and n_2 respectively, we calculate their modified NtD map $\tilde{\mathcal{N}}$ and modified magnetic TtL operator $\tilde{\mathcal{M}}$, then establish the nonlinear equation (1), where $\boldsymbol{\phi}$ represents $\tilde{\phi}_x^{\pm}$ and $\tilde{\phi}_y^{\pm}$ on the two line segments (of length 0.5μm) separating Ω_1 and Ω_2, and $\tilde{\phi}_x$ on the boundary of the waveguide.

At the frequency corresponding to a free space wavelength $\lambda = 2\pi/k_0 = 1.5\mu$m, we calculate the propagation constant β for a few values of the graded mesh order p and for different number of discretization points. For

the first case ($n_1 = 1.5$), Chiang *et al.* [23] obtained an accurate solution $\beta/k_0 = \underline{1.27627403}771648$ based on a Legendre pseudospectral penalty method. Using $p = 8$ and $N_F = 1946$, where N_F is the size (row or column numbers) of the square matrix F as in the nonlinear eigenvalue problem (1), we obtain a reference solution $\beta/k_0 = 1.2762740378358$. Notice that first ten digits of these two solutions are identical. Using our reference solution, we calculate the absolute errors for other numerical solutions obtained using smaller values of p and N_F. The results are shown in Fig. 3 in a logarithmic

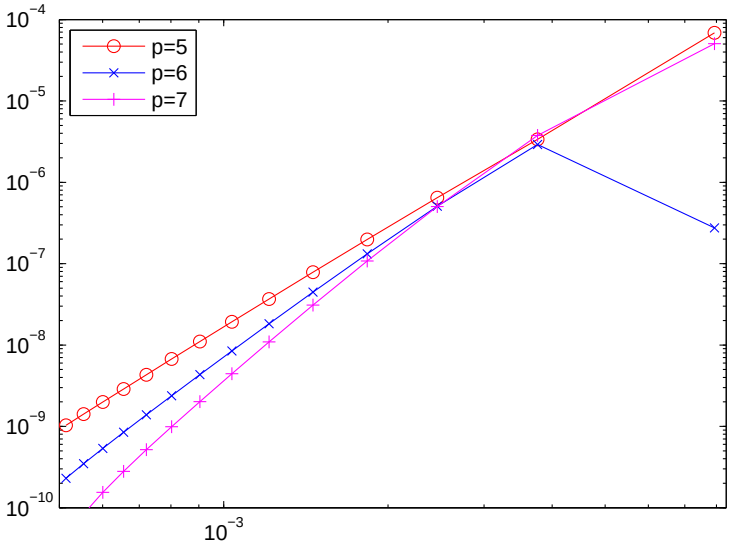

Figure 3: Dependence of the absolute error on the inverse of the matrix size of F for the bounded waveguide shown in Fig. 2(a) and $n_1 = 1.5$.

scale, where the vertical axis is the absolute error and the horizontal axis is N_F^{-1}. To estimate the order of accuracy of our numerical method, we calculate local slopes based on two nearby solutions for each curve in Fig. 3. The results are given in Table 1 (columns 2-4). For this case, our method appears to have at least a $(p-1)$-th order of accuracy. For the second case ($n_1 = \sqrt{8}$), we obtain a reference solution $\beta/k_0 = 2.65679692423851$ using $p = 8$ and $N_F = 1946$ and it agrees with Hadley's result $\beta/k_0 = \underline{2.65679692} \pm 10^{-8}$ given in [8]. In Fig. 4, we show the absolute errors for numerical solutions corresponding to small values of p and N_F. Approximate orders of accuracy are given in Table 1 (columns 5-7). Apparently, the orders are lower than

Matrix size N_F	$n_1 = 1.5$			$n_1 = \sqrt{8}$		
	$p = 5$	$p = 6$	$p = 7$	$p = 5$	$p = 6$	$p = 7$
546, 686	4.05	4.75	5.46	3.37	4.75	5.05
686, 826	4.09	4.84	5.62	3.42	4.11	5.10
826, 966	4.11	4.90	5.74	3.44	4.15	5.15
966, 1106	4.13	4.96	5.85	3.46	4.18	5.23
1106, 1246	4.15	5.01	5.96	3.48	4.22	5.34
1246, 1386	4.17	5.06	6.12	3.50	4.27	5.52
1386, 1526	4.19	5.13	6.36	3.52	4.32	5.83

Table 1: Approximate orders of accuracy for the waveguide shown in Fig. 2(a), estimated from two solutions of different matrix size N_F and a reference solution.

those of the first case. Even for a fixed p, the order of our method may depend on the regularity of the electromagnetic field at the corners. The higher index-contrast of the second case gives rise to stronger corner singularities which could reduce the order of our method.

Next, we consider three open waveguides each consisting of a high-index core and a homogeneous surrounding medium. These waveguides have a square core, an isosceles trapezoidal core and a drop-shaped core as shown in Fig. 2(b), Fig. 1(a) and Fig. 2(c), respectively. The square waveguide was previously analyzed by Hadley [8] and by Lu and Yevick [38]. The size of the square core is $1\mu\text{m} \times 1\mu\text{m}$ and its refractive index is $n_1 = \sqrt{8}$. The trapezoidal waveguide is another example considered by Lu and Yevick [38]. The height and the length of the top edge of the isosceles trapezoidal core are both $1\mu\text{m}$, its base angle is 80° and its refractive index is $n_1 = \sqrt{8}$. The boundary of the drop-shaped core is given by the following parametric representation

$$\boldsymbol{r}(\gamma) = \left(\sqrt{3}\sin\frac{\gamma}{2}, -\frac{1}{2}\sin\gamma\right), \quad 0 \le \gamma \le 2\pi,$$

where the unit is μm, and it refractive index is $n_1 = 3.4$. For all three waveguides, the medium surrounding the core is air ($n_2 = 1$). We calculate the propagation constant β at a frequency with a corresponding free space wavelength $\lambda = 1.5\mu\text{m}$. Using $p = 8$ and $N_F = 2224$, two reference solutions $\beta/k_0 = 2.65679553054187$ and $\beta/k_0 = 2.68364294770014$ are obtained for the square and trapezoidal waveguides, respectively. Up to the first six digits, our result for the square waveguide agrees with the result of Hadley

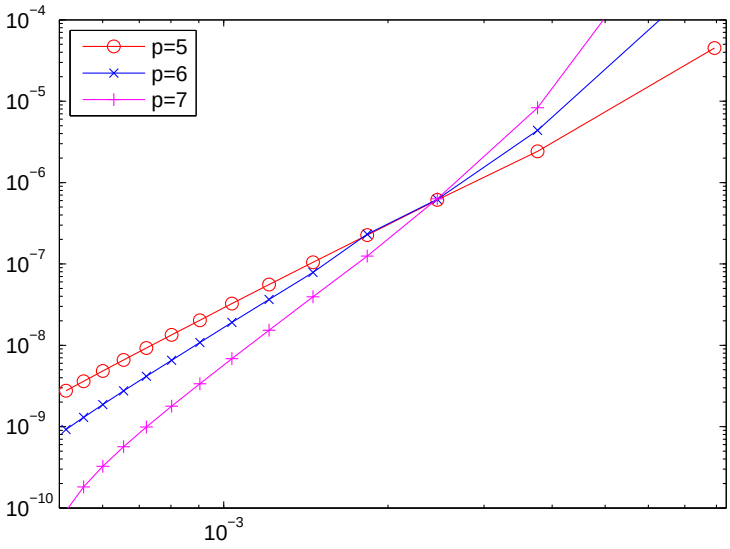

Figure 4: Dependence of the absolute error on the inverse of the matrix size of F for the bounded waveguide shown in Fig. 2(a) and $n_1 = \sqrt{8}$.

[8] (2.6567969) and the result of Lu and Yevick [38] (2.6567937). For the trapezoidal waveguide, Lu and Yevick [38] used a small computational window of $2\,\mu$m$\times 2\,\mu$m, and their result (2.6254) does not agree with ours. Using these two reference solutions, we calculate the absolute errors of other numerical solutions corresdponding to small values of p and N_F. The results are shown in Fig. 5 and Fig. 6 for the square and trapezoidal waveguides, respectively. In Table 2, we show the approximate orders of accuracy for these two waveguides. For the drop-shaped waveguide shown in Fig. 2(c), we obtain a reference solution $\beta/k_0 = 3.273944841352$ using $p = 7$ and $N_F = 1996$. The absolute errors of other numerical solutions for this waveguide are shown in Fig. 7. The approximate orders of accuracy for this waveguide is given in Table 3 (columns 1-4).

Finally, we consider a rectangular waveguide where the background is a layered medium as shown in Fig. 1(b). The waveguide has a 0.5μm $\times$ 0.22μm rectangular core with a refractive index $n_1 = 3.5$ and a two-layer background with refractive indices $n_2 = 1$ and $n_3 = 1.45$. It corresponds to a silicon wire on a SiO_2 substrate. This waveguide is a related to a structure studied by a number of groups in [52]. Their structure has a finite SiO_2 layer (of

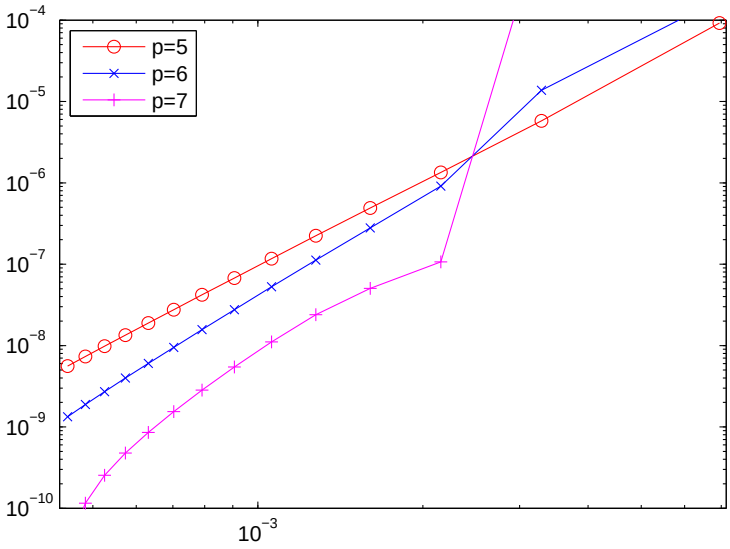

Figure 5: Dependence of the absolute error on the inverse of the matrix size of F for the square waveguide shown in Fig. 2(b).

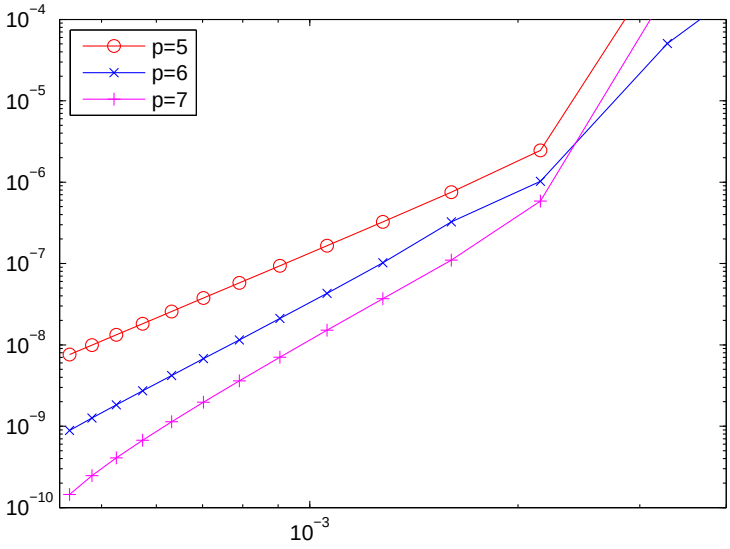

Figure 6: Dependence of the absolute error on the inverse of the matrix size of F for the trapezoidal waveguide shown in Fig. 1(a).

Matrix size N_F	Square waveguide			Trapezoidal waveguide		
	$p=5$	$p=6$	$p=7$	$p=5$	$p=6$	$p=7$
624, 784	3.45	4.00	3.25	3.69	5.09	4.78
784, 944	3.48	4.07	4.14	3.63	4.66	4.80
944, 1104	3.50	4.12	4.54	3.61	4.53	4.89
1104, 1264	3.51	4.17	4.83	3.60	4.48	4.97
1264, 1424	3.53	4.21	5.12	3.59	4.47	5.07
1424, 1584	3.54	4.23	5.53	3.59	4.47	5.20
1584, 1744	3.56	4.32	6.07	3.59	4.49	5.41

Table 2: Approximate orders of accuracy estimated from two solutions of different matrix size N_F and a reference solution, for the square and trapzoidal waveguides shown in Fig. 2(b) and Fig. 1(a), respectively.

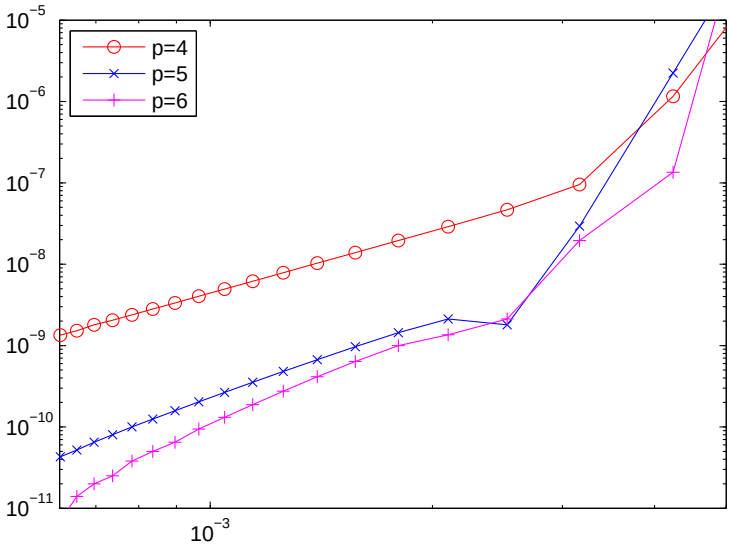

Figure 7: Dependence of the absolute error on the inverse of the matrix size of F for the drop-shaped waveguide shown in Fig. 2(c).

Drop-shaped waveguide				Rectangular waveguide			
N_F	$p=4$	$p=5$	$p=6$	N_F	$p=4$	$p=5$	$p=6$
636, 796	2.53	3.06	3.62	1320, 1512	1.30	4.06	5.85
796, 956	2.54	3.12	3.77	1512, 1704	1.66	3.87	6.14
956, 1116	2.54	3.13	3.92	1704, 1896	1.86	3.70	6.45
1116, 1276	2.54	3.07	3.12	1896, 2088	1.98	3.57	6.80
1276, 1436	2.39	3.10	3.60	2088, 2280	2.06	3.46	7.18
1436, 1596	2.81	3.09	4.56	2280, 2472	2.12	3.38	7.63

Table 3: Approximate orders of accuracy estimated from two solutions of different matrix size N_F and a reference solution, for the drop-shaped waveguide shown in Fig. 2(c) and rectangular waveguide shown in Fig. 1(b).

thickness 1μm) and a lower silicon substrate with the same refractive index as the core. It is a leaky waveguide for which the propagation constant β is complex. However, the real part of their β should be quite close to our β. We calculate the guided mode of this rectangular waveguide for free space wavelength $\lambda = 1.55\mu$m. To formulate the nonlinear eigenvalue problem (1), we need to calculate the relevant operators for the three domains Ω_1, Ω_2 and Ω_3 corresponding to the refractive indices n_1, n_2 and n_3, where Ω_2 and Ω_3 are unbounded. Since the interface between the two background media extends to infinity, it is necessary to truncate Ω_2 and Ω_3. On the external boundaries of the truncated domains in the upper and lower half-planes, we assume that $\partial_{\boldsymbol{\nu}} H_x$ and $\partial_{\boldsymbol{\nu}} H_y$ are zero. Of course, the numerical solutions now depend on the size of the truncated domains. Since the electromagnetic field of a guided mode decays exponentially away from the core, the above truncation process is feasible in practice. For a truncated domain corresponding to $|x| < 1.45\mu$m on the x-axis, we calculate the propagation constant for $4 \leq p \leq 7$ and for different values of N_F. These numerical solutions converge to $\beta/k_0 = 2.41237200$. This agrees with the best result (2.412372) given in [52]. In Fig. 8, we show the dependence of the absolute errors of the numerical solutions on the size of the matrix F. In Table 3 (columns 5-8), we show the estimated orders of accuracy. The size of the truncated domain appears to be sufficiently large. In fact, on a smaller truncated domain corresponding to $|x| < 1.05\mu$m, we obtain solutions with the same first 7 digits (i.e., 2.412372). It is relatively difficult to obtain an accurate solution for this waveguide, since we need six interior segments to formulate the nonlinear eigenvalue problem and the size of matrix F increases rapidly as the number of points on each

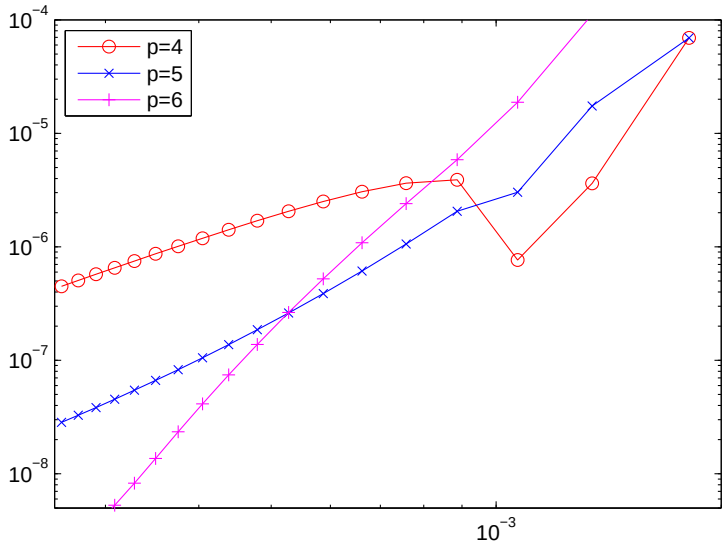

Figure 8: Dependence of the absolute error on the inverse of the matrix size of F for the rectangular waveguide with a layered background shown in Fig. 1(b).

segment is increased. When N_F is large, the problem becomes ill-conditioned, in the sense that the matrix F is nearly singular even if β is not close to a propagation constant. In that case, the round-off errors set a limit on the obtainable accuracy of the numerical solutions.

7. Conclusion

In this paper, we developed a new full-vectorial boundary integral equation method for computing guided modes of optical waveguides. The method is applicable to waveguides with high index-contrast, sharp corners and layered background. The integral equations are used to compute the Neumann-to-Dirichlet operators for sub-domains of constant refractive index on the transverse plane of the waveguide, and they are discretized by a Nyström method with a graded mesh for handling the corners. Unlike previous full-vectorial boundary integral equation formulations based on the two longitudinal components, we use the normal derivatives of the two transverse components of the magnetic field as the basic unknown functions. For waveguides with corners, general mode solvers with high order of accuracy are difficult to

find, since the electromagnetic fields diverge at the corners. The performance of our method depends on the graded mesh order p and also on the problem, possibly due to the different field singularities at different corners. In general, a larger p gives a higher order of accuracy. For the examples studied in this paper, we have obtained sufficiently accurate solutions for $4 \leq p \leq 8$.

References

[1] A. W. Snyder and J. D. Love, *Optical Waveguide Theory*, Chapman and Hall, London, 1983.

[2] D. Marcuse, *Theory of Dielectric Optical Waveguides*, 2nd ed., Academic Press, Boston, 1991.

[3] C. Vassallo, *Optical Waveguide Concepts*, Elsevier, Amsterdam, 1991.

[4] K. Bierwirth, N. Schulz, and F. Arndt, Finite-difference analysis of rectangular dielectric wave-guide structures, IEEE Trans. Microwave Theory Tech. 34 (1986) 1104-1114.

[5] H. A. Jamid and M. N. Akram, A new higher order finite-difference approximation scheme for the method of lines, J. Lightwave Technol. 19 (2001) 398-404.

[6] N. N. Feng, G. R. Zhou, C. L. Xu, W. P. Huang, Computation of full-vector modes for bending waveguide using cylindrical perfectly matched layers, J. Lightwave Technol. 20 (2002) 1976-1980.

[7] G. R. Hadley, High-accuracy finite-difference equations for dielectric waveguide analysis I: Uniform regions and dielectric interfaces, J. Lightwave Technol. 20 (2002) 1210-1218.

[8] G. R. Hadley, High-accuracy finite-difference equations for dielectric waveguide analysis II: Dielectric corners, J. Lightwave Technol. 20 (2002) 1219-1231.

[9] C. P. Yu and H. C. Chang, Yee-mesh-based finite difference eigenmode solver with PML absorbing boundary conditions for optical waveguides and photonic crystal fibers, Opt. Express 12 (2004) 6165-6177.

[10] M. Wik, D. Dumas, and D. Yevick, Comparison of vector finite-difference techniques for modal analysis, J. Opt. Soc. Am. A 22 (2005) 1341-1347.

[11] N. Thomas, P. Sewell, T. M. Benson, A new full-vectorial higher order finite-difference scheme for the modal analysis of rectangular dielectric waveguides, J. Lightwave Technol. 25 (2007) 2563-2570.

[12] Y. P. Chiou, Y. C. Chiang, C. H. Lai, C. H. Du, and H. C. Chang, Finite difference modeling of dielectric waveguides with corners and slanted facets, J. Lightwave Technol. 27 (2009) 2077-2086.

[13] B. M. A. Rahman and J. B. Davies, Finite-element solution of integrated optical wave-guides, J. Lightwave Technol. **2** (1984) 682-688.

[14] M. Koshiba, K. Hayata, and M. Suzuki, Vectorial finite-element method without spurious solutions for dielectric waveguide problems, Electronics Letters 20 (1984) 409-410.

[15] Z.-E. Abid, K. L. Johnson, and A. Gopinath, Analysis of dielectric guides by vector tranverse magnetic field finite elements, J. Lightwave Technol. 11 (1993) 1545-1549.

[16] M. Koshiba, S. Maruyama, and K. Hirayama, A vector finite-element method with the high-order mixed-interpolation-type triangular elements for optical wave-guiding problems, J. Lightwave Technol. 12 (1994) 495-502.

[17] M. Koshiba and Y. Tsuji, Curvilinear hybrid edge/nodal elements with triangular shape for guided-wave problems, J. Lightwave Technol. 18 (2000) 737-743.

[18] S. Selleri, L. Vincetti L, A. Cucinotta, and M. Zoboli, Complex FEM modal solver of optical waveguides with PML boundary conditions, Opt. Quant. Electron. 33 (2001) 359-371.

[19] S. S. A. Obayya, B. M. A. Rahman, K. T. V. Grattan, and H. A. El-Mikati, Full vectorial finite-element-based imaginary distance beam propagation solution of complex modes in optical waveguides, J. Lightwave Technol. 20 (2002) 1054-1060.

[20] J. H. Yuan, An adaptive inverse iteration FEM for the inhomogeneous dielectric waveguides, Journal of Computational Mathematics 25 (2007) 169-184.

[21] C. C. Huang, C. C. Huang, and J. Y. Yang, A full-vectorial pseudospectral modal analysis of dielectric optical waveguides with stepped refractive index profiles, IEEE Journal of Selected Topics in Quantum Electronics 11 (2005) 457-465.

[22] P. J. Chiang, C. L. Wu, C. H. Teng, C. S. Yang, and H. C. Chang, Full-vectorial optical waveguide mode solvers using multidomain pseudospectral frequency-domain (PSFD) formulations, IEEE Journal of Quantum Electronics 44 (2008) 56-66.

[23] S. F. Chiang, B. Y. Lin, C. H. Teng, and H. C. Chang, Improved analysis of rectangular dielectric waveguides based on a Legendre pseudospectral penalty scheme, Integrated Photonics Research, Silicon and Nano Photonics on CDROM, paper IWH8, The Optical Society, Washington, DC, 2010.

[24] R. Mittra, Y. L. Hou, and V. Jamnejad, Analysis of open dielectric waveguides using mode-matching technique and variational-methods, IEEE Trans. Microwave Theory Tech. 28 (1980) 36-43.

[25] S. T. Peng and A. A. Oliner, Guidance and leakage properties of a class of open dielectric waveguides: mathematical formulations, IEEE Trans. Microwave Theory Tech. 29 (1981) 843-855.

[26] A. S. Sudbo, Numerically stable formulation of the transverse resonance method for vector mode-field calculations in dielectric waveguides, IEEE Photon. Technol. Lett. 5 (1993) 342-344.

[27] A. S. Sudbo, Improved formulation of the film mode matching method for mode field calculations in dielectric waveguides, Pure and Appl. Opt. 3 (1993) 381-388.

[28] L. Prkna, M. Hubalek, and J. Ctyroky, Vectorial eigenmode solver for bent waveguides based on mode matching IEEE Photon. Technol. Lett. 16 (2004) 2057-2059.

[29] W. Wijngaard, Guided normal modes of two parallel circular dielectric rods, J. Opt. Soc. Am. 63 (1973) 944-949.

[30] E. Yamashita, S. Ozeki, and K. Atsuki, Modal analysis method for optical fibers with symmetrically distributed multiple cores, J. Lightwave Technol. 3 (1985) 341-346.

[31] K. M. Lo, R. C. McPhedran, I. M. Bassett, and G. W. Milton, An electromagnetic theory of dielectric waveguides with multiple embedded cylinders, J. Lightwave Technol. 12 (1994) 396-410.

[32] C. S. Chang and H. C. Chang, Theory of the circular harmonics expansion method for multiple-optical-fiber system, J. Lightwave Technol. 12 (1994) 415-417.

[33] T. P. White, B. T. Kuhlmey, R. C. McPhedran, D. Maystre, G. Renversez, C. M. de Sterke, and L. C. Botten, Multipole method for microstructured optical fibers. I. Formulation, J. Opt. Soc. Am. B 19 (2002) 2322-2330.

[34] B. T. Kuhlmey, T. P. White, G. Renversez, D. Maystre, L. C. Botten, C. M. de Sterke, and R. C. McPhedran, Multipole method for microstructured optical fibers. II. Implementation and results, J. Opt. Soc. Am. B 19 (2002) 2331-2340.

[35] L. Wang, J. A. Cox, and A. Friedman, Model analysis of homogeneous optical waveguides by the boundary integral formulation and the Nyström method, J. Opt. Soc. Am. A 15 (1998) 92-100.

[36] S. V. Boriskina, T. M. Benson, P. Sewell, and A.I. Nosich, Highly efficient full-vectorial integral equation solution for the bound, leaky, and complex modes of dielectric waveguides, IEEE J. of Selected Topics in Quantum Electron, 8 (2002) 1225-1232.

[37] T. Lu, D. Yevick, A vectorial boundary element method analysis of integrated optical waveguides, J. Lightwave Technol. 21 (2003) 1793-1807.

[38] T. Lu, D. Yevick, Comparative evaluation of a novel series approximation for electromagnetic fields at dielectric corners with boundary element method applications, J. Lightwave Technol. 22 (2004) 1426-1432.

[39] H. Cheng, W. Y. Crutchfield, M. Doery, and L. Greengard, Fast, accurate integral equation methods for the analysis of photonic crystal fibers I: Theory, Opt. Express 12 (2004) 3791-3805.

[40] E. Pone, A. Hassani, S. Lacroix, A. Kabashin, and M. Skorobogatiy, Boundary integral method for the challenging problems in bandgap guiding, plasmonics and sensing, Opt. Express 15 (2007) 10231-10246.

[41] C. Bouwcamp, A note on singularities occurring at sharp edges in electromagnetic diffraction theory, Physica 12 (1946) 467.

[42] J. Meixner, The behavior of electromagnetic fields at edges, IEEE Trans. Antennas Propag. AP-20 (1972) 442-446.

[43] G. I. Makarov and A. V. Osipov, Structure of Meixner's series, Radiophys. Quantum Electron. 29 (1986) 544-549.

[44] A. S. Sudbo, Why are accurate computations of mode fields in rectangular dielectric waveguides difficult?, J. Lightwave Technol. 10 (1992) 418-419.

[45] Y. Wu and Y. Y. Lu, Analyzing diffraction gratings by a boundary integral equation Neumann-to-Dirichlet map method, J. Opt. Soc. Am. B 26 (2009) 2444-2451.

[46] D. Colton and R. Kress, *Inverse Acoustic and Electromagnetic Scattering Theory*, 2nd ed., Springer-Verlag, Berlin, 1998.

[47] E. Martensen, Über eine methode zum räumlichen neumannschen problem mit einer anwendung für torusartige berandungen, Acta Math. 109 (1963) 75-135.

[48] R. Kussmaul, Ein numerisches verfahren zur lösung des Neumannschen aussenraumproblems für die Helmholtzsche schwingungsgleichung, Computing 4 (1969) 246-273.

[49] R. Kress, A Nyström method for boundary integral equations in domains with corners, Numer. Math. 58 (1990) 145-161.

[50] Y. Jeon, A Nyström method for boundary integral equations in domains with a piecewise smooth boundary, Journal of Integral Equations and Applications, 5 (1993) 221-242.

[51] A. Hochman and Y. Leviatan, Efficient and spurious-free integral-equation-based optical waveguide mode solver, Opt. Express 15 (2007) 14431-14453.

[52] P. Bienstman, S. Selleri *et al.* Modelling leaky photonic wires: A mode solver comparison, Opt. Quant. Electron. 38 (2006) 731-759.